Electronic Supplementary Materials
Control of functionalized single-walled carbon nanotube photoluminescence via competition between thermal rearrangement and elimination

Yutaka Maeda,[a,*] Rina Morooka,[a] Pei Zhao,[b,*] Michio Yamada,[a] Masahiro Ehara[b,*]

[a] Department of Chemistry, Tokyo Gakugei University, Tokyo 184-8501, Japan

[b] Research Center for Computational Science, Institute for Molecular Science, Okazaki 444-8585, Japan

Experimental

Fig. S1 (a) Raman (561 nm excitation), (b) absorption, (c) PL spectra (567 nm excitation) of SWNTs (black), SWNTs-$C_3H_4Me_2$ (red), SWNTs-$C_3H_4Me_2$ (200 ˚C, 6 h) (orange), SWNTs-$C_3H_4Me_2$ (300 ˚C, 6 h) (green), SWNTs-$C_3H_4Me_2$ (400 ˚C) (blue), and SWNTs-$C_3H_4Me_2$ (400 ˚C, 6 h) (purple). Functionalized SWNTs were dispersed in D_2O solution containing 1 wt% SDBS for absorption and PL measurements.

Fig. S2 HPLC profiles of functionalized SWNTs and gradient proportion of DOC (%). Conditions: column, ϕ 10 mm × 200 mm; eluent, H_2O containing 0.5 wt.% of SC, 0.5 wt.% of SDS, and X wt.% of DOC, where X corresponds to the values shown on the gradient; flow rate, 2 mL/min; and detection, absorption at 280 nm.

Fig. S3 Normalized absorption spectra of the separated SWNTs-C_3H_6 before and after thermal treatment dispersed in a D_2O solution containing 1 wt% SC. Black line: SWNTs-C_3H_6. Red line: SWNTs-C_3H_6 (300 ˚C). Blue line: SWNTs-C_3H_6 (400 ˚C). The DOC concentration of each fraction and peak assignment are shown in each spectrum.

Fig. S4 Absorption spectra of the separated SWNTs-C_3H_6 before and after thermal treatment dispersed in a D_2O solution containing 1 wt% SC. The DOC concentration of each fraction and peak assignment are shown in each spectrum.

Fig. S5 Absorption spectra of the separated SWNTs-C_3H_6 (350˚C) before and after thermal treatment dispersed in a D_2O solution containing 1 wt% SC. The DOC concentration of each fraction and peak assignment are shown in each spectrum.

Fig. S6 Absorption spectra of the separated SWNTs-C_3H_6 (400 ˚C) before and after thermal treatment dispersed in a D_2O solution containing 1 wt% SC. The DOC concentration of each fraction and peak assignment are shown in each spectrum.

Fig. S7 Normalized absorption spectra of the separated SWNTs-$C_3H_4Me_2$ before and after thermal treatment dispersed in a D_2O solution containing 1 wt% SC. Black line: SWNTs-$C_3H_4Me_2$. Red line: SWNTs-$C_3H_4Me_2$ (300 ˚C, 6 h). Blue line: SWNTs-$C_3H_4Me_2$ (400 ˚C, 6 h). The DOC concentration of each fraction and peak assignment are shown in each spectrum.

Fig. S8 Absorption spectra of the separated SWNTs-$C_3H_4Me_2$ before and after thermal treatment dispersed in a D_2O solution containing 1 wt% SC. The DOC concentration of each fraction and peak assignment are shown in each spectrum.

Fig. S9 Absorption spectra of the separated SWNTs-$C_3H_4Me_2$ (300 ˚C, 6 h) before and after thermal treatment dispersed in a D_2O solution containing 1 wt% SC. The DOC concentration of each fraction and peak assignment are shown in each spectrum.

Fig. S10 Absorption spectra of the separated SWNTs-$C_3H_4Me_2$ (400 ˚C, 6 h) before and after thermal treatment dispersed in a D_2O solution containing 1 wt% SC. The DOC concentration of each fraction and peak assignment are shown in each spectrum.

Fig. S11 Raman spectra (633 nm excitation) of SWNTs-C_3H_6 (red), SWNTs-C_3H_6 (350 ˚C) (green), and SWNTs-C_3H_6 (400 ˚C) (green).

Fig. S12 Raman spectra (561 nm excitation) of SWNTs-C_3H_6 (red), SWNTs-C_3H_6 (350 ˚C) (green), and SWNTs-C_3H_6 (400 ˚C) (green).

Fig. S13 Raman spectra (633 nm excitation) of SWNTs-$C_3H_4Me_2$ (red), SWNTs-$C_3H_4Me_2$ (200 ˚C, 6 h) (yellow), SWNTs-$C_3H_4Me_2$ (300 ˚C, 6 h) (green), SWNTs-$C_3H_4Me_2$ (400 ˚C, 6 h) (blue), and SWNTs-$C_3H_4Me_2$ (400 ˚C) (purple).

Fig. S14 Raman spectra (561nm excitation) of SWNTs-$C_3H_4Me_2$ (red), SWNTs-$C_3H_4Me_2$ (200 ˚C, 6 h) (yellow), SWNTs-$C_3H_4Me_2$ (300 ˚C, 6 h) (green), SWNTs-$C_3H_4Me_2$ (400 ˚C, 6 h) (blue), and SWNTs-$C_3H_4Me_2$ (400 ˚C) (purple).

Fig. S15 Absorption and CD spectra of separated SWNTs-C_3H_6 (DOC: 0.027, 0.034), and SWNTs-C_3H_6 (350 ˚C) (DOC: 0.027, 0.034) in D_2O containing 1wt% SC. CD spectra were normalized by the E_{22} absorbance. D/G values in each sample are shown in the figure.

Fig. S16 Absorption and CD spectra of separated SWNTs-$C_3H_4Me_2$ (DOC: 0.027, 0.034) and SWNTs-$C_3H_4Me_2$ (300 ˚C, 6 h) (DOC: 0.029, 0.034) in D_2O containing 1wt% SC. CD spectra were normalized by the E_{22} absorbance. D/G values in each sample are shown in the figure.

Fig. S17 PL mapping of SWNTs-C_3H_6 (350 ˚C) dispersed in D_2O containing 1 wt.% SC.

Fig. S18 PL mapping of SWNTs-C_3H_6 (400 ˚C) dispersed in D_2O containing 1 wt.% SC.

Fig. S19 PL mapping of SWNTs-$C_3H_4Me_2$ dispersed in D_2O containing 1 wt.% SC.

Fig. S20 PL mapping of SWNTs-$C_3H_4Me_2$ (200 ˚C, 6h) dispersed in D_2O containing 1 wt.% SC.

Fig. S21 PL mapping of SWNTs-$C_3H_4Me_2$ (300 ˚C, 6h) dispersed in D_2O containing 1 wt.% SC.

Fig. S22 PL mapping of SWNTs-$C_3H_4Me_2$ (400 ˚C) dispersed in D_2O containing 1 wt.% SC.

Fig. S23 PL mapping of SWNTs-$C_3H_4Me_2$ (400 ˚C, 6 h) dispersed in D_2O containing 1 wt.% SC.

Fig. S24 Partial view of the optimized structures of SWNTs-$C_3H_4Me_2$ at the level of B3LYP/6-31G*.

Fig. S25 Calculated transition energy difference between the functionalized and non-functionalized SWNTs (∆transition energy) as a function of the squared diameter of SWNTs. 1,2-L_{++} binding configuration (red). 1,2-L_{+} binding configuration (black). 1,2-L_{-} binding configuration (blue). *trans*-(6,4) SWNTs-$C_3H_4Me_2$ (●). *trans*-(6,5) SWNTs-$C_3H_4Me_2$ (▲). *trans*-(8,3) SWNTs-$C_3H_4Me_2$ (▼). *trans*-(7,5) SWNTs-$C_3H_4Me_2$ (◆).

Table S1. Relative energies (ΔE, in kcal/mol), transition energies (in eV/nm), and oscillator strength (*f*) of SWNTs-$C_3H_4Me_2$.

Complete reference list

Ref 35: Frisch, M. J.; Trucks, G. W.; Schlegel, H. B.; Scuseria, G. E.; Robb, M. A.; Cheeseman, J. R.; Scalmani, G.; Barone, V.; Mennucci, B.; Petersson, G. A.; Nakatsuji, H.; Caricato, M.; Li, X.; Hratchian, H. P.; Izmaylov, A. F.; Bloino, J.; Zheng, G.; Sonnenberg, J.L.; Hada, M.; Ehara, M.; Toyota, K.; Fukuda, R.; Hasegawa, J.; Ishida, M.; Nakajima, T.; Honda, Y.; Kitao, O.; Nakai, H.; Vreven, T.; Montgomery Jr., J. A.; Peralta, J. E.; Ogliaro, F.; Bearpark, M.; Heyd, J. J.; Brothers, E.; Kudin, K. N.; Staroverov, V. N.; Kobayashi, R.; Normand, J.; Raghavachari, K.; Rendell, A.; Burant, J. C.; Iyengar, S. S.; Tomasi, J.; Cossi, M.; Rega, N.; Millam, J. M.; Klene, M.; Knox, J. E.; Cross, J. B.; Bakken, V.; Adamo, C.; Jaramillo, J.; Gomperts, R.; Stratmann, R. E.; Yazyev, O.; Austin, A. J.; Cammi, R.; Pomelli, C.; Ochterski, J. W.; Martin, R. L.; Morokuma, K.; Zakrzewski, V. G.; Voth, G. A.; Salvador, P.; Dannenberg, J. J.; Dapprich, S.; Daniels, A. D.; Farkas, O.; Foresman, J. B.; Ortiz, J. V.; Cioslowski, J.; Fox, D. J. Gaussian 09, Revision E.01, Gaussian, Inc., Wallingford CT, **2013**.

Experimental

General

The (6,5)-enriched SWCNTs (SG 65i) used in this work was purchased from Sigma-Aldrich. Reagent-grade naphthalene, sodium, DOC, SC and SDBS were purchased from commercial suppliers. For the reactions with SWCNTs, tetrahydrofuran (THF) (Super Plus, Kanto Chemical Co., INC) was purified using a Glass Contour solvent dispensing system (Nikko-Hansen & Co., Ltd), and ethanol was dried over Mg prior to use. Thermal treatment of the samples was performed at a heating rate of 10°C/min and a nitrogen flow rate of 50 mL/min (TG-50A; Shimadzu Corp.). The samples were held for 30 min at 100°C for drying. Optical absorption spectra were recorded using a spectrophotometer (V-670; Jasco Corp.) equipped with a Pyrex cell with a 10 mm path length. The SWCNT adducts were dispersed in D_2O containing 1 wt% of SDBS by ultrasound irradiation in a bath-type sonicator at an ultrasonic frequency of 42 kHz with 100 W power (B2510J-MT ultrasonic cleaner; Branson) and centrifuged at 140000 g for 1 h in a high-speed centrifuge equipped with an S58A angle rotor (micro ultracentrifuge CS 100FNX; Koki Holdings Co., Ltd.). To adjust the absorption intensity of SWNTs and functionalized SWNTs before separation to approximately 778 nm, an adequate dose of D_2O solution containing 1 wt% SDBS was added to the dispersion, depending on the concentration. The resulting diluted dispersion was used for PL measurements. The NIR fluorescence intensity as a function of the excitation and emission wavelengths of the dispersed SWCNTs was obtained using a spectrophotometer equipped with a 450 W lamp and a Symphony-II CCD detector (Nanolog; HORIBA Ltd.). For the separated SWNTs, the absorption spectra shown in Figure S4-S11 were used for PL measurements.

General procedure for the preparation of functionalized SWNTs.

Naphthalene (300 mg, 2.34 mmol) and sodium (156 mg, 6.79 mmol) were put in a 200 mL heat-dried three-necked round-bottom flask under argon. Thereafter, anhydrous tetrahydrofuran (100 mL) was added to the flask and the mixture was stirred for 60 min. A portion (10.0 mg) of SWNTs was put in a 200 mL heat-dried three-necked round-bottom flask under argon. Sodium naphthalenide solution was added to the SWNTs, which were thereafter sonicated for 60 min, and bromoalkene or dibromoalkane (6.8 mmol) was subsequently added to the mixture. The mixture was sonicated for 30 min and thereafter quenched by adding 4 mL of dry ethanol. The resulting suspended black solid was collected through filtration using a membrane filter (PTFE, 1.0 μm) and washed with tetrahydrofuran, methanol, and acetone via the dispersion-filtration process.

Preparation of 2,4-dibromopentane.

2,4-pentanediol (48.0 mmol, 4.9 g) was dissolved in dichloromethane (50 mL) in a dry flask under Ar atmosphere. The solution was cooled to -15˚, and phosphorus tribromide (52.6 mmol, 14.2 g) was added dropwise with stirring. The mixture was stirred for 2 hours at 0˚C and for 21 h at room temperature. Water (50 mL) was added and the product extracted with dichloromethane (20 mL x 3) was washed with cold water (20 mL x 5). The organic layer was dried over anhydrous sodium sulfate. It was purified by distillation and 2,4-dibromopentane was corrected as mixture of stereoisomer at 120˚C / 12 mmHg as colorless liquid. (2.5 g, 10.8 mmol, 23%)

(2R, 4R)-2,4-dibromopentane: ^{1}H NMR (400 MHz, $CDCl_3$) δ ＝1.72 (d, J=7.3 Hz, 6H), 2.17 (dt, J=6.9Hz, 14.7 Hz, 1H), 2.51 (dt, J=7.8Hz, 14.7 Hz, 1H), 4.20 (sext, J=6.9 Hz, 2H); ^{13}C NMR (100 MHz, $CDCl_3$) δ＝25.6, 47.4, 51.7. **(2R, 4S)-2,4-dibromopentane:** ^{1}H NMR (400 MHz, $CDCl_3$) δ＝ 1.77 (d, J=6.9 Hz, 6H), 2.10 (dd, J=5.5 Hz, 1.8 Hz, 2H), 4.37 (sext, J=6.4 Hz, 2H); ^{13}C NMR (100 MHz, $CDCl_3$) δ＝ 26.7, 50.0, 51.8.

Separation of functionalized SWNTs.

Approximately 4.0 mg of functionalized SWNTs were added to a vial containing 5 mL of aqueous 1 wt% sodium cholate (SC) (≥98%, TCI Co., Ltd). The vial was sonicated for 3 h (Sonics & Materials Inc., Ultrasonic Processor VCX750). The resulting dispersion was centrifuged at 210,000 × *g* for 1 h. Thereafter, 2 mL of 2 wt% sodium dodecyl sulfate (SDS, ≥97%, TCI Co., Ltd.) was added to 2 mL of the supernatant solution before HPLC separation. The helicity sorting of the SWNTs was achieved via

HPLC using a JASCO ChromNAV system equipped with a JASCO LC-Net II interface, JASCO PU-2089i gradient inert pump, JASCO MD-4010 photodiode array detector, and column (ϕ10 mm × 200 mm) filled with a gel (Sephacryl S-200, Cytiva) at ~23 ˚C. The flow rate was 2.0 mL min^{-1} and the sample (SWNTs dispersion) injection volume was 3 mL. The eluent was an aqueous solution containing 0.5 wt.% SC + 0.5 wt.% SDS + X wt.% sodium deoxycholate (DOC, ≥96%, FUJIFILM Wako Pure Chemical Co.). The concentration of DOC (X) was increased from 0 to 0.058 wt.% according to a previous study.[1-4] Fractions were collected every 2.5 min using a fraction collector (Super Fraction Collector SF-2120, Advantec Toyo Kaisha, Ltd.).

Theoretical details

One-unit cell of (8,3), and (7,5) SWNTs was adopted for the computational models, while two-unit cell was constructed for (6,4) SWNT. The dangling bonds at the terminals were passivated with hydrogen atoms or a mixture of hydrogen atoms and two methylene groups to eliminate mid-gap trap states. We performed geometric optimizations at the level of B3LYP/6-31G* for SWNTs-$C_3H_4Me_2$, and applied B3LYP/3-21G for time dependent DFT (TD-DFT) calculations. The most stable adducts were obtained by considering possible positions for the two methyl groups. All DFT calculations were performed using the Gaussian 09 suite of the program version E.01.

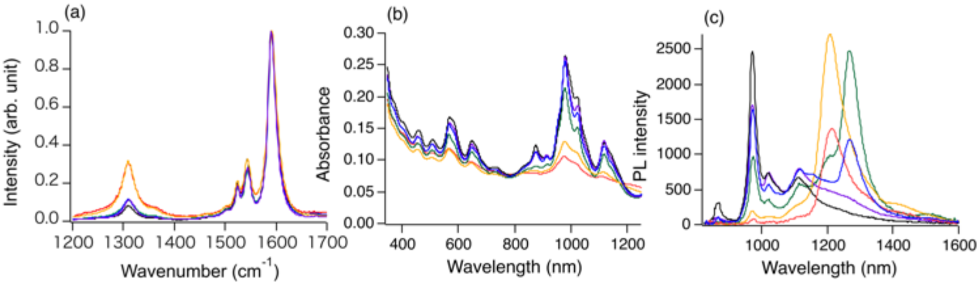

Fig. S1 (a) Raman (561 nm excitation), (b) absorption, (c) PL spectra (567 nm excitation) of SWNTs (black), SWNTs-$C_3H_4Me_2$ (red), SWNTs-$C_3H_4Me_2$ (200 ˚C, 6 h) (orange), SWNTs-$C_3H_4Me_2$ (300 ˚C, 6 h) (green), SWNTs-$C_3H_4Me_2$ (400 ˚C) (blue), and SWNTs-$C_3H_4Me_2$ (400 ˚C, 6 h) (purple). Functionalized SWNTs were dispersed in D_2O solution containing 1 wt% SDBS for absorption and PL measurements.

Separation of SWNT adducts.

The chromatographic separation of SWNTs-$C_3H_4Me_2$ before and after the thermal treatment was conducted by gradient of sodium deoxycholate (DOC) concentration in the eluent using high-performance liquid chromatography (HPLC) with Sephacryl S-200 as the stationary phase (Fig. S2).[24-26] The separated fraction was replaced with D_2O containing 1 wt% sodium cholate (SC) for absorption and PL analysis in the NIR region. Functionalization of SWNTs using 1,3-dibromopropane to afford the corresponding adducts (SWNTs-C_3H_6) and the thermal treatment and HPLC separation of the adducts were also performed as a control experiment. The chiral index assignment of separated SWNTs was conducted by using the characteristic absorption and PL peak wavelengths, as well as the radial breathing mode (RBM) peaks of Raman spectra (Figure S3–S16).

Figure S7 depicts the absorption spectra of the separated SWNTs-$C_3H_4Me_2$ before and after thermal treatment; these were selected for analysis of PL characteristics. The assignment of the chiral index in each fraction was confirmed by the wavelength of the characteristic E_{11} and E_{22} absorption peaks.[27] Although there was a slight difference in composition of the included SWNT chirality in each fraction, six chiral SWNTs-$C_3H_4Me_2$ were assigned by the absorption spectra. The elution order with increasing DOC concentration was (6,4), (7,3), (6,5), (8,3), (7,5), and (8,4) SWNTs. The highly pure (6,5) SWNTs were observed in the fraction of DOC concentration from 0.027 to 0.034 (Figs. S3–S10.). The circular dichroism (CD) spectra of these fractions showed the mirror-image CD spectra similar to those of (11,-5) and (6,5) SWNTs,[28,29] demonstrating that optical resolution is achieved for the functionalized (6,5) SWNTs (Fig. S15 and S16). The solution phase Raman spectra support the assignment of their chiral index. The RBM peaks observed at 307 and 335 cm^{-1} with 561 nm excitation and at 282 and 298 cm^{-1} with 633 nm excitation were assigned to the RBM peaks of (6,5), (6,4), (7,5), and (8,3) SWNTs, respectively (Figs. S11–S14).[27] A similar separation behavior was observed for SWNTs-C_3H_6 and SWNTs-$C_3H_4Me_2$ before and after the thermal treatment.

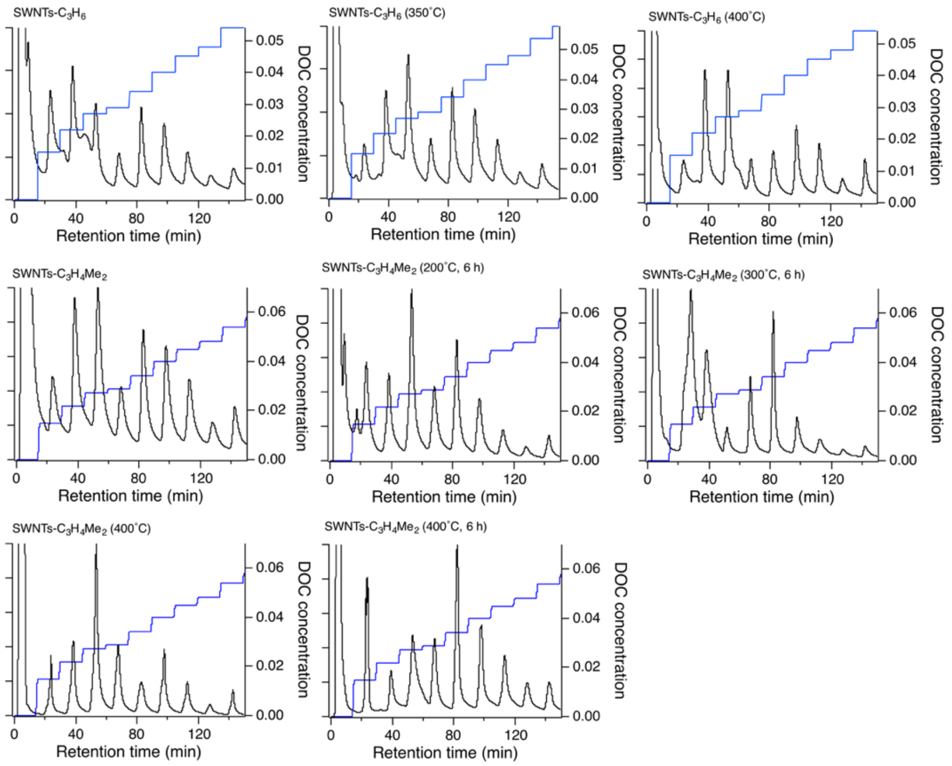

Fig. S2 HPLC profiles of functionalized SWNTs and gradient proportion of DOC (%). Conditions: column, ϕ 10 mm × 200 mm; eluent, H_2O containing 0.5 wt.% of SC, 0.5 wt.% of SDS, and X wt.% of DOC, where X corresponds to the values shown on the gradient; flow rate, 2 mL/min; and detection, absorption at 280 nm.

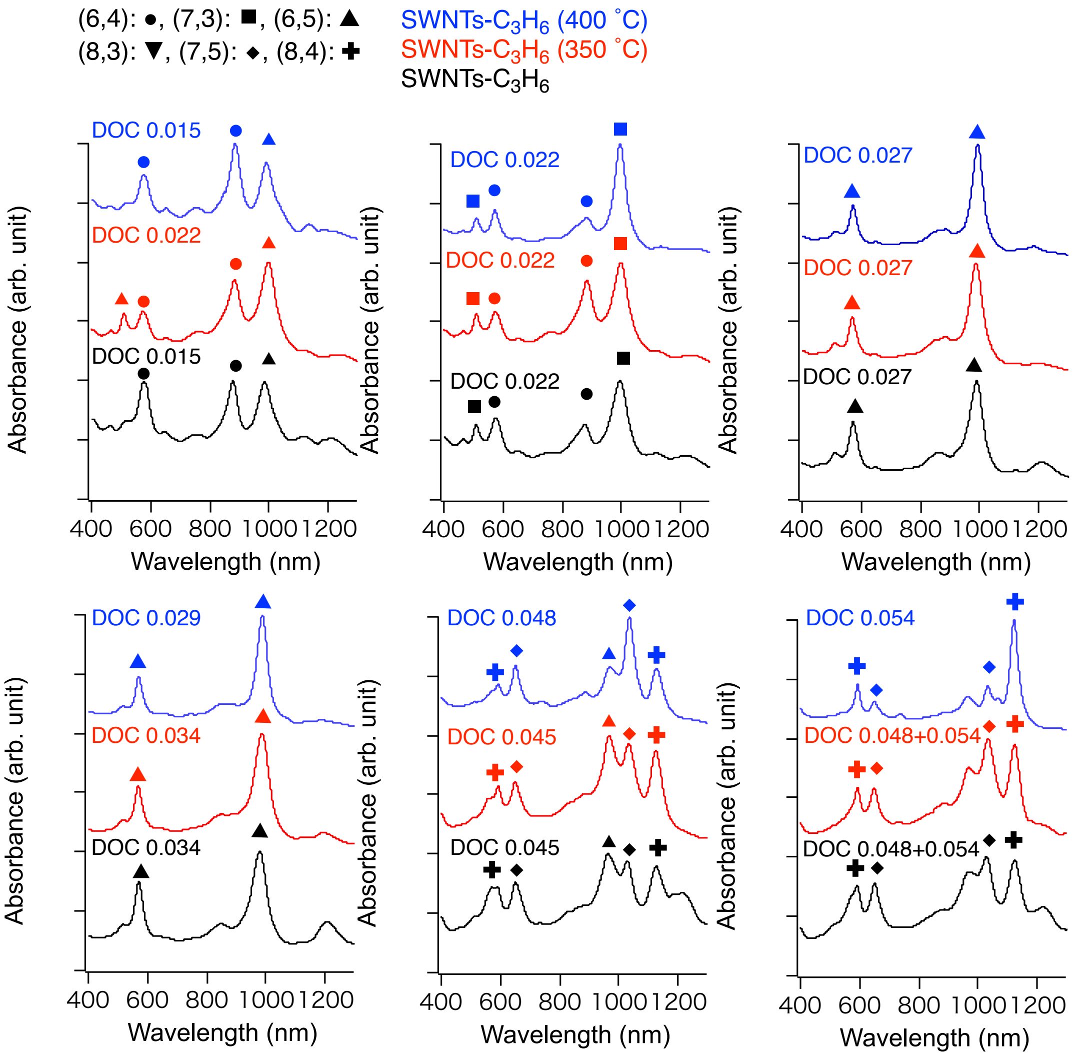

Fig. S3 Normalized absorption spectra of the separated SWNTs-C_3H_6 before and after thermal treatment dispersed in a D_2O solution containing 1 wt% SC. Black line: SWNTs-C_3H_6. Red line: SWNTs-C_3H_6 (300 ˚C). Blue line: SWNTs-C_3H_6 (400 ˚C). The DOC concentration of each fraction and peak assignment are shown in each spectrum.

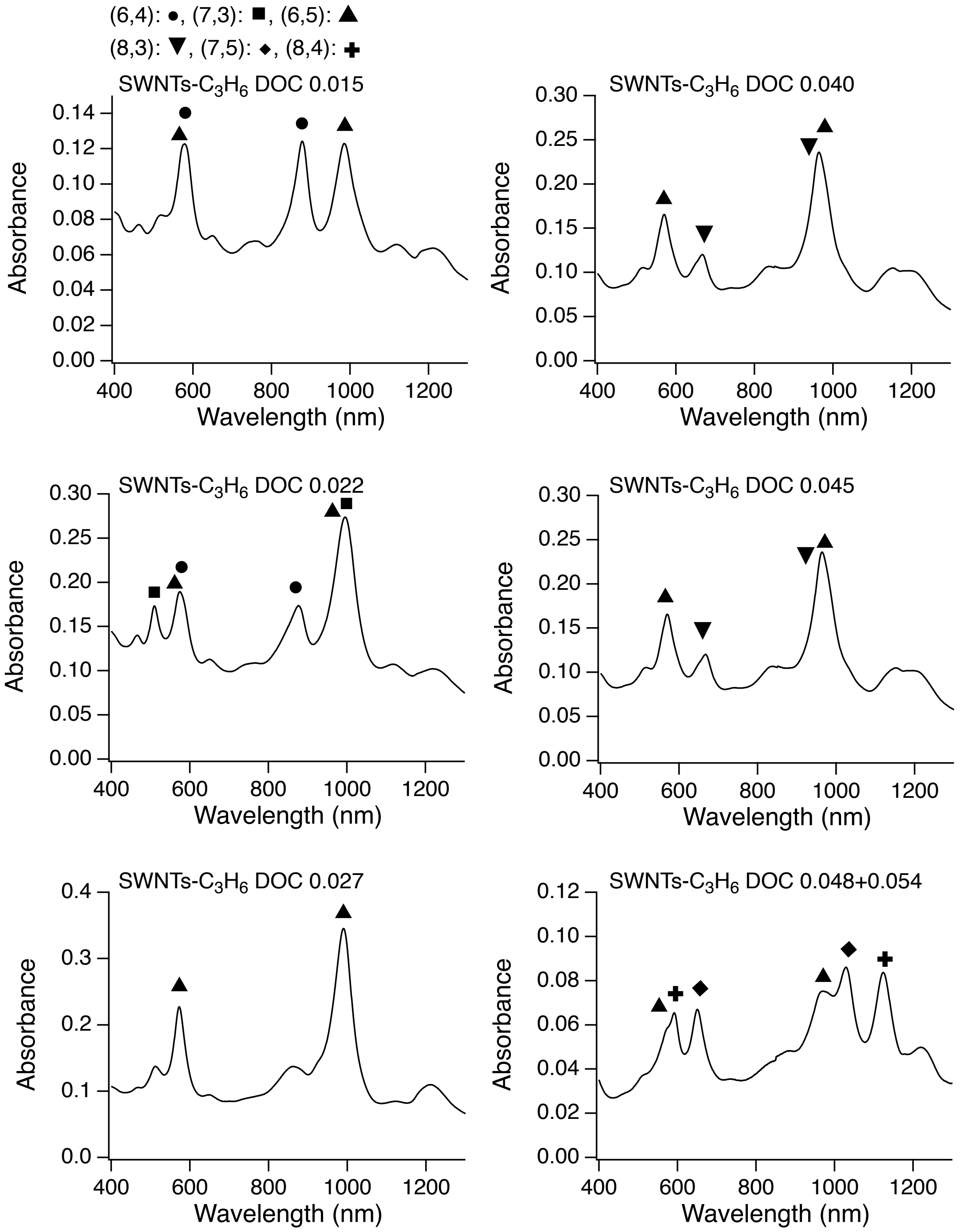

Fig. S4 Absorption spectra of the separated SWNTs-C_3H_6 before and after thermal treatment dispersed in a D_2O solution containing 1 wt% SC. The DOC concentration of each fraction and peak assignment are shown in each spectrum.

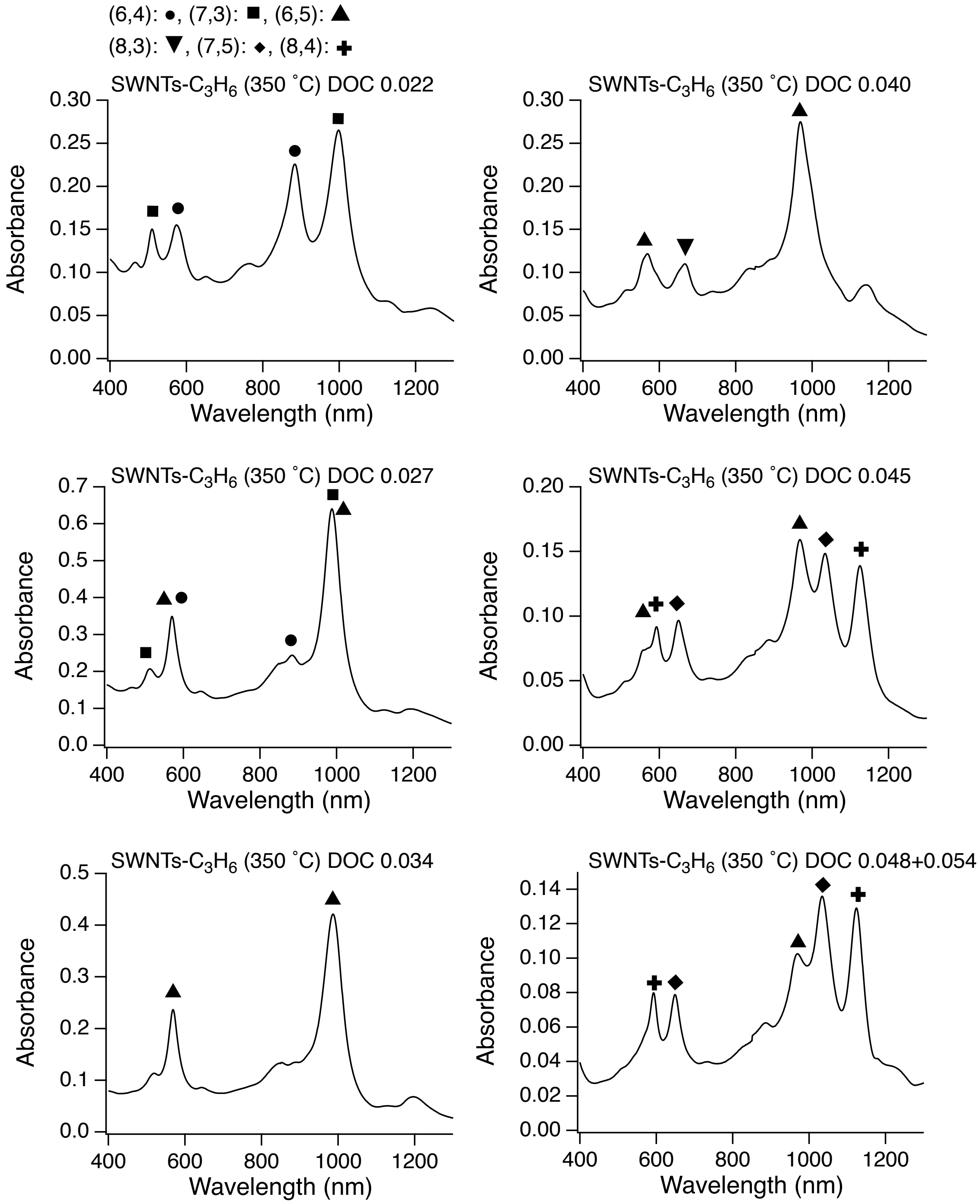

Fig. S5 Absorption spectra of the separated SWNTs-C_3H_6 (350˚C) before and after thermal treatment dispersed in a D_2O solution containing 1 wt% SC. The DOC concentration of each fraction and peak assignment are shown in each spectrum.

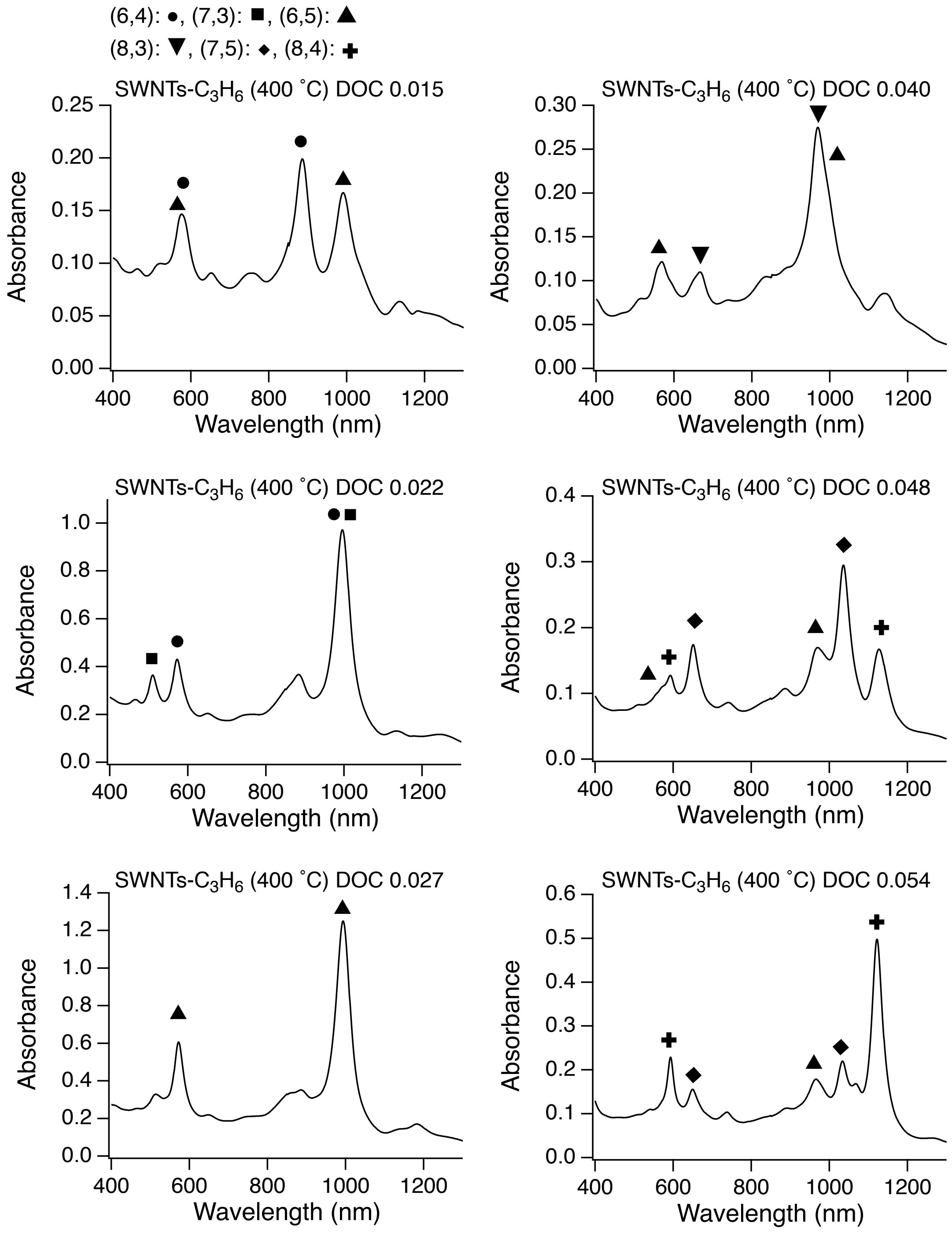

Fig. S6 Absorption spectra of the separated SWNTs-C_3H_6 (400 ˚C) before and after thermal treatment dispersed in a D_2O solution containing 1 wt% SC. The DOC concentration of each fraction and peak assignment are shown in each spectrum.

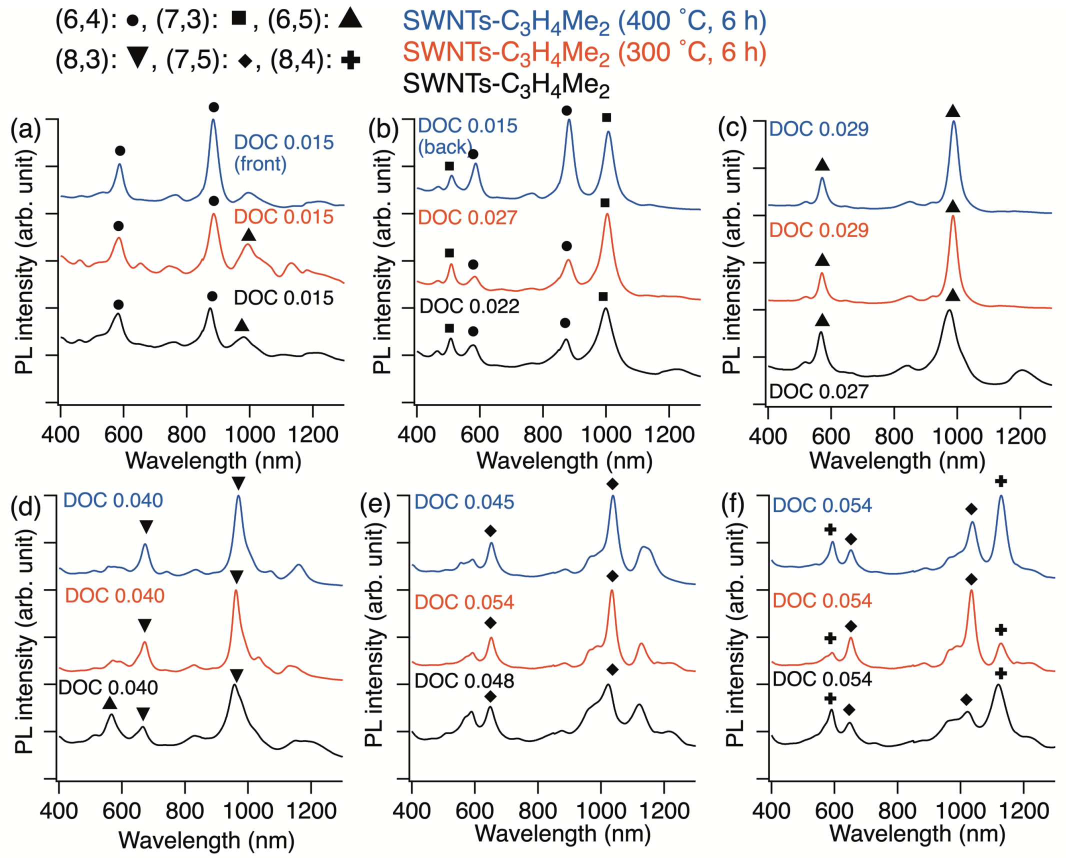

Fig. S7 Normalized absorption spectra of the separated SWNTs-$C_3H_4Me_2$ before and after thermal treatment dispersed in a D_2O solution containing 1 wt% SC. Black line: SWNTs-$C_3H_4Me_2$. Red line: SWNTs-$C_3H_4Me_2$ (300 ˚C, 6 h). Blue line: SWNTs-$C_3H_4Me_2$ (400 ˚C, 6 h). The DOC concentration of each fraction and peak assignment are shown in each spectrum.

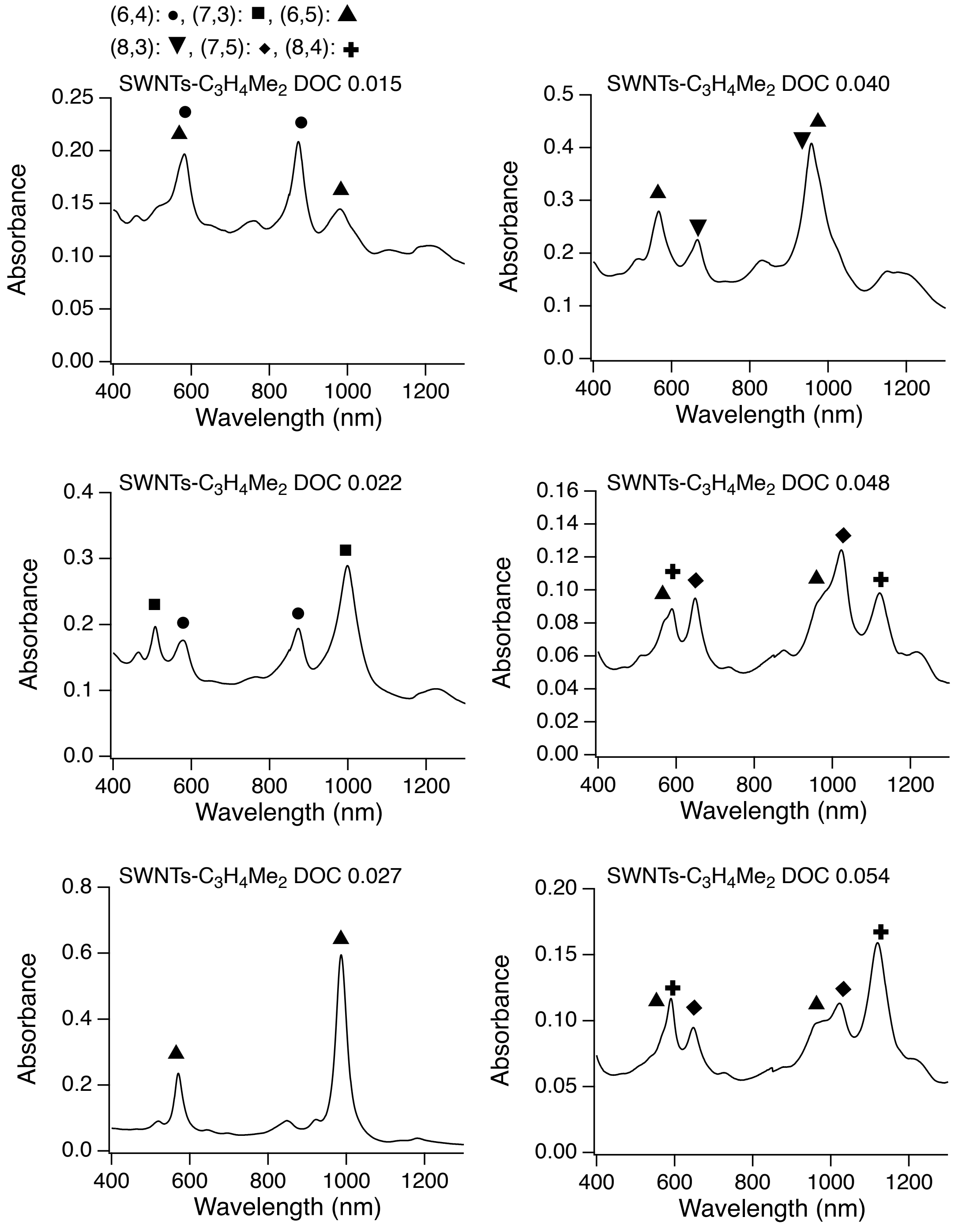

Fig. S8 Absorption spectra of the separated SWNTs-$C_3H_4Me_2$ before and after thermal treatment dispersed in a D_2O solution containing 1 wt% SC. The DOC concentration of each fraction and peak assignment are shown in each spectrum.

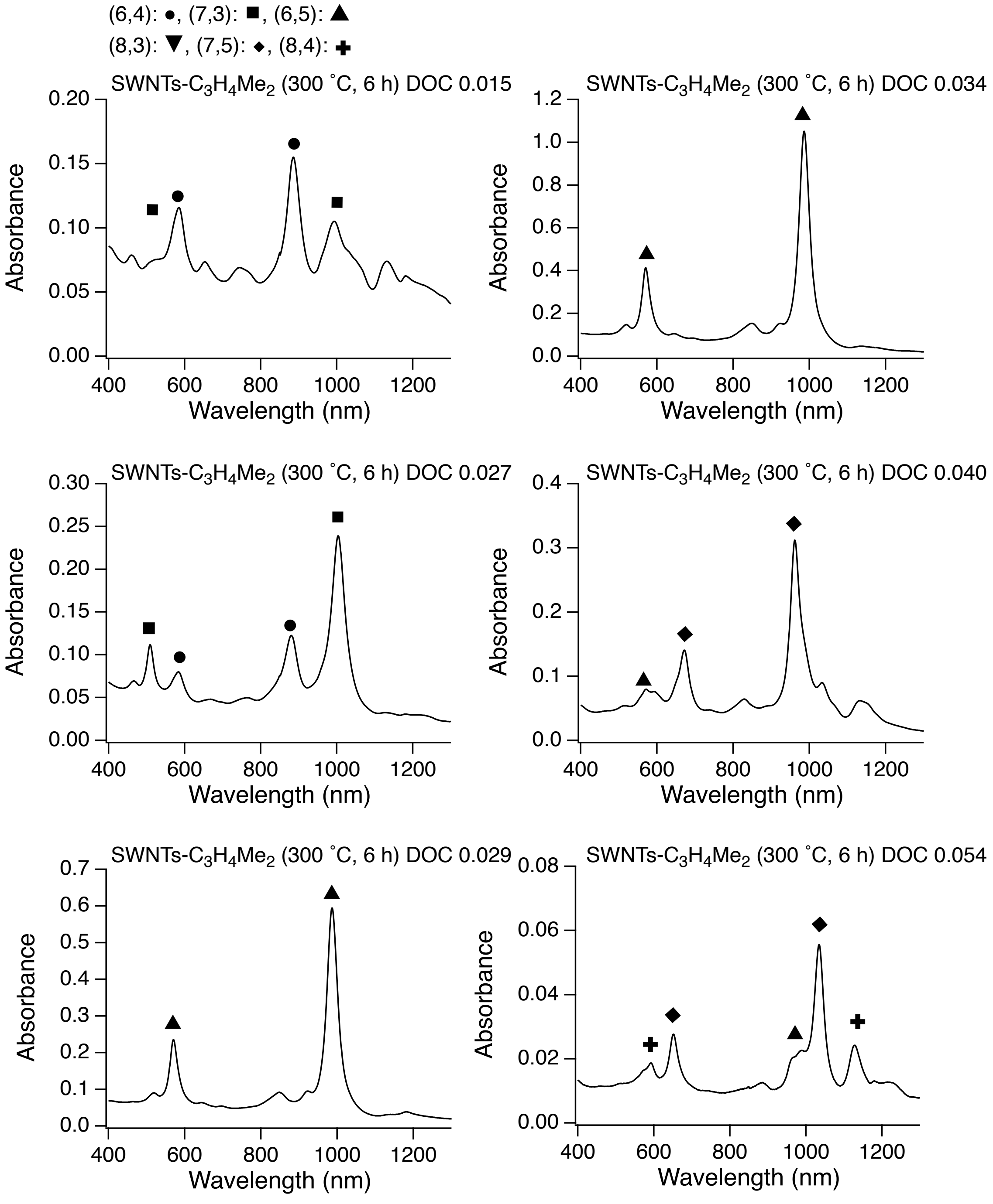

Fig. S9 Absorption spectra of the separated SWNTs-$C_3H_4Me_2$ (300 ˚C, 6 h) before and after thermal treatment dispersed in a D_2O solution containing 1 wt% SC. The DOC concentration of each fraction and peak assignment are shown in each spectrum.

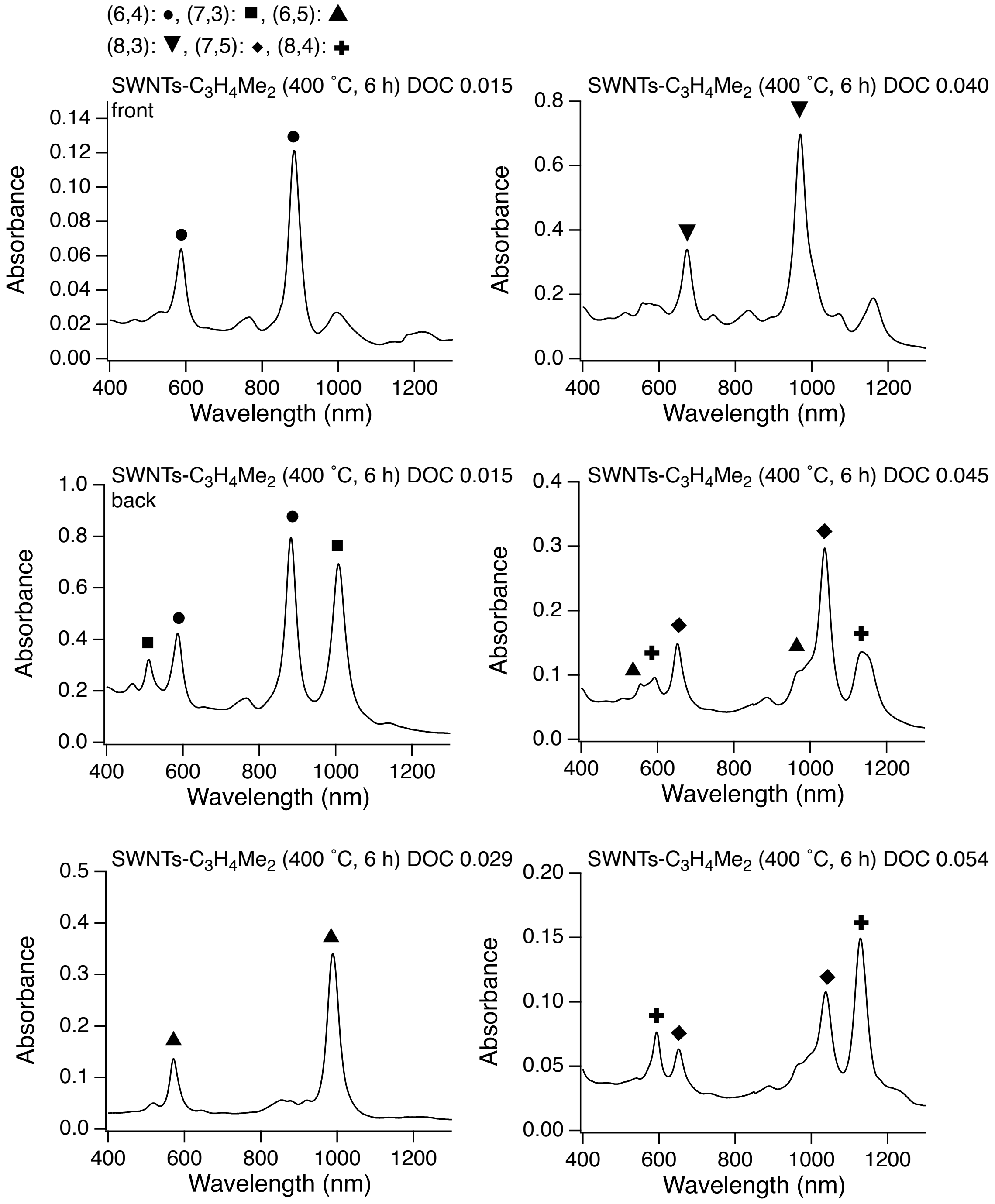

Fig. S10 Absorption spectra of the separated SWNTs-$C_3H_4Me_2$ (400 ˚C, 6 h) before and after thermal treatment dispersed in a D_2O solution containing 1 wt% SC. The DOC concentration of each fraction and peak assignment are shown in each spectrum.

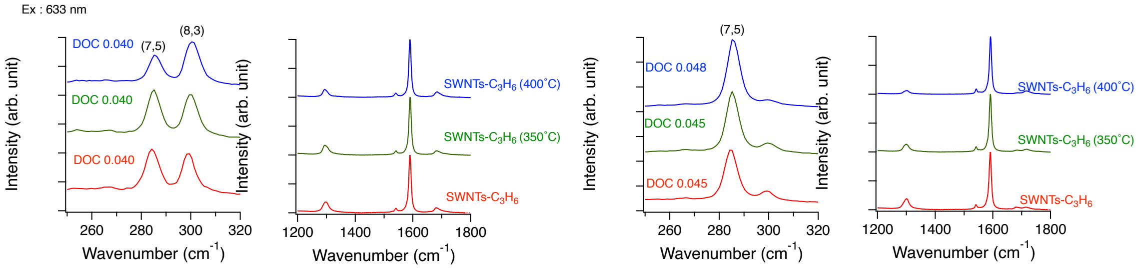

Fig. S11 Raman spectra (633 nm excitation) of SWNTs-C_3H_6 (red), SWNTs-C_3H_6 (350 ˚C) (green), and SWNTs-C_3H_6 (400 ˚C) (green).

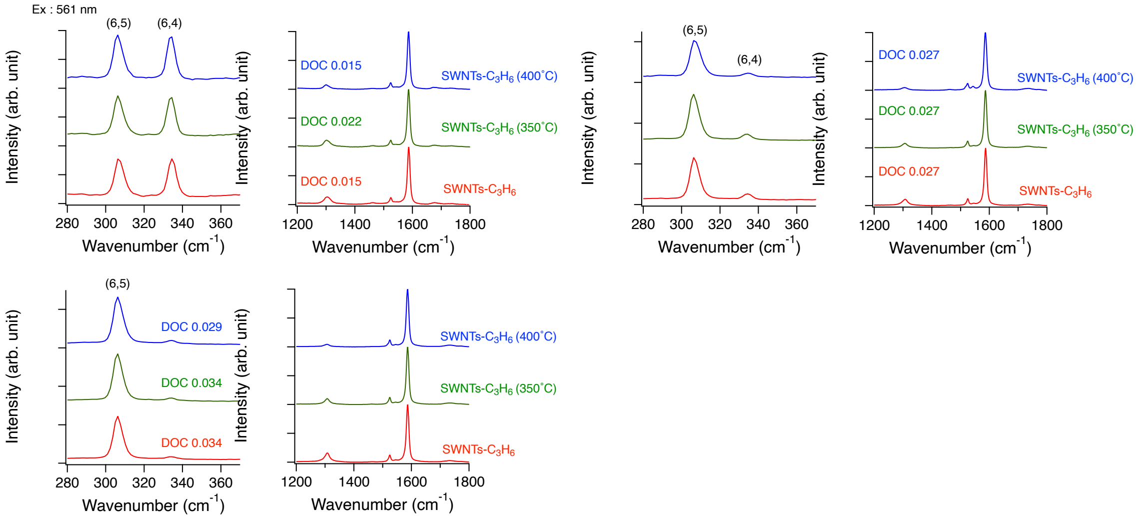

Fig. S12 Raman spectra (561 nm excitation) of SWNTs-C_3H_6 (red), SWNTs-C_3H_6 (350 ˚C) (green), and SWNTs-C_3H_6 (400 ˚C) (green).

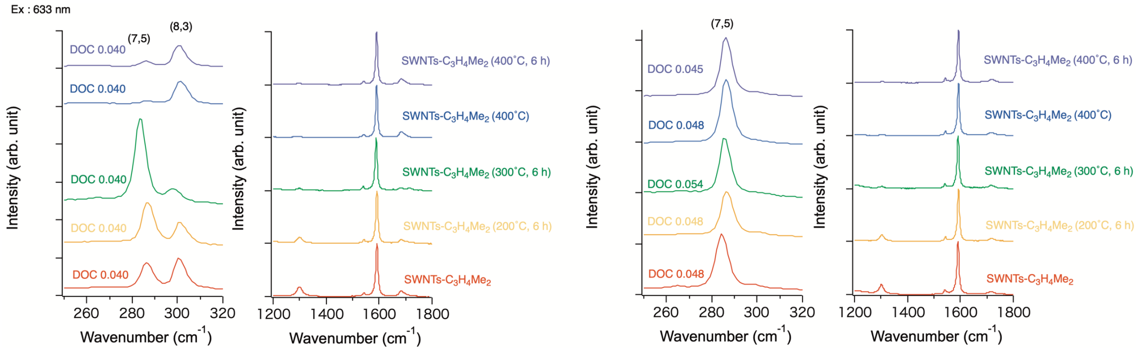

Fig. S13 Raman spectra (633 nm excitation) of SWNTs-$C_3H_4Me_2$ (red), SWNTs-$C_3H_4Me_2$ (200 ˚C, 6 h) (yellow), SWNTs-$C_3H_4Me_2$ (300 ˚C, 6 h) (green), SWNTs-$C_3H_4Me_2$ (400 ˚C, 6 h) (blue), and SWNTs-$C_3H_4Me_2$ (400 ˚C) (purple).

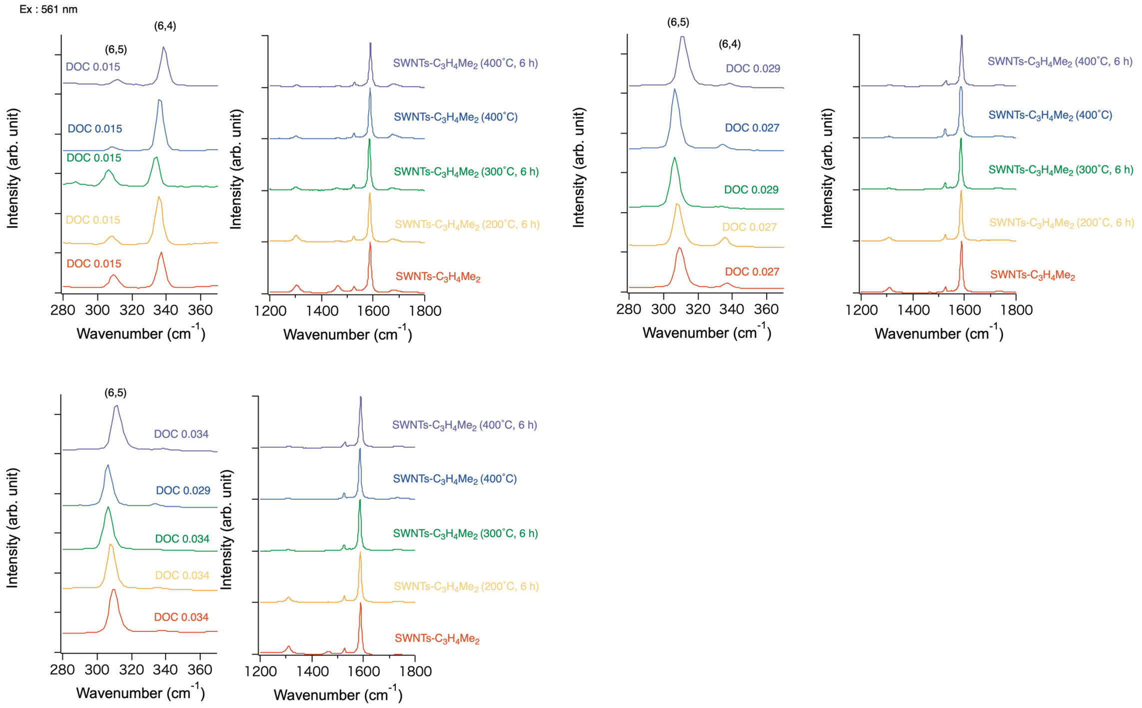

Fig. S14 Raman spectra (561nm excitation) of SWNTs-$C_3H_4Me_2$ (red), SWNTs-$C_3H_4Me_2$ (200 ˚C, 6 h) (yellow), SWNTs-$C_3H_4Me_2$ (300 ˚C, 6 h) (green), SWNTs-$C_3H_4Me_2$ (400 ˚C, 6 h) (blue), and SWNTs-$C_3H_4Me_2$ (400 ˚C) (purple).

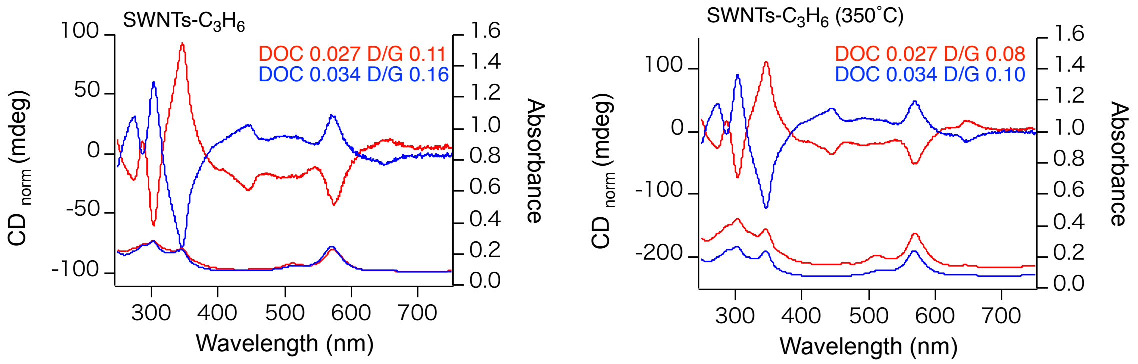

Fig. S15 Absorption and CD spectra of separated SWNTs-C_3H_6 (DOC: 0.027, 0.034), and SWNTs-C_3H_6 (350 ˚C) (DOC: 0.027, 0.034) in D_2O containing 1wt% SC. CD spectra were normalized by the E_{22} absorbance. D/G values in each sample are shown in the figure.

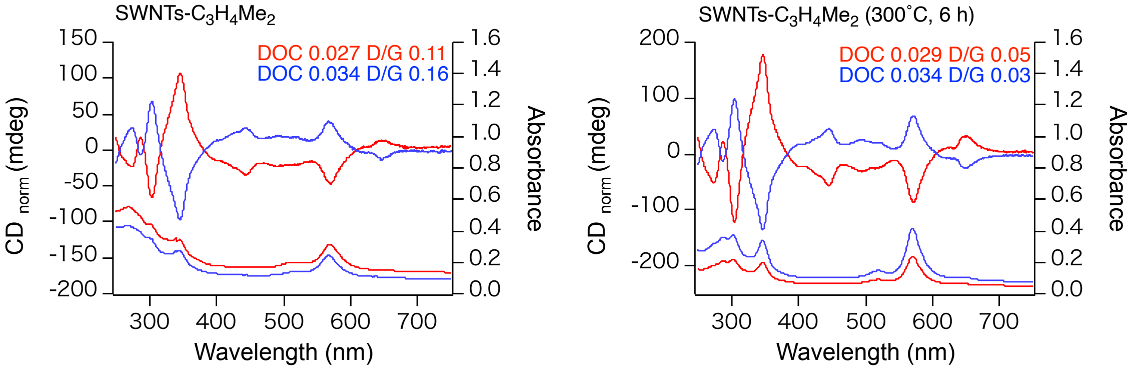

Fig. S16 Absorption and CD spectra of separated SWNTs-$C_3H_4Me_2$ (DOC: 0.027, 0.034) and SWNTs-$C_3H_4Me_2$ (300 ˚C, 6 h) (DOC: 0.029, 0.034) in D_2O containing 1wt% SC. CD spectra were normalized by the E_{22} absorbance. D/G values in each sample are shown in the figure.

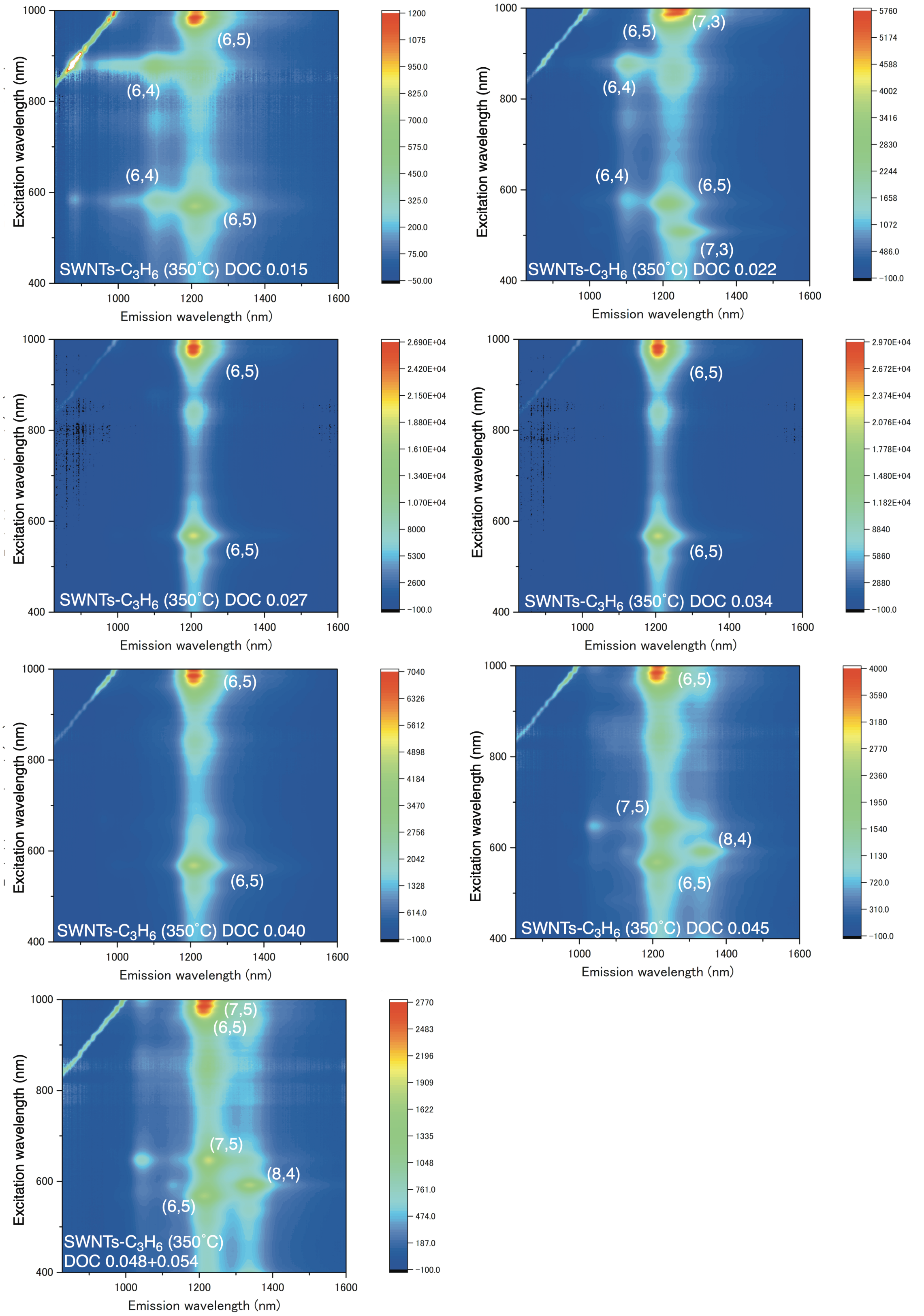

Fig. S17 PL mapping of SWNTs-C_3H_6 (350 ˚C) dispersed in D_2O containing 1 wt.% SC.

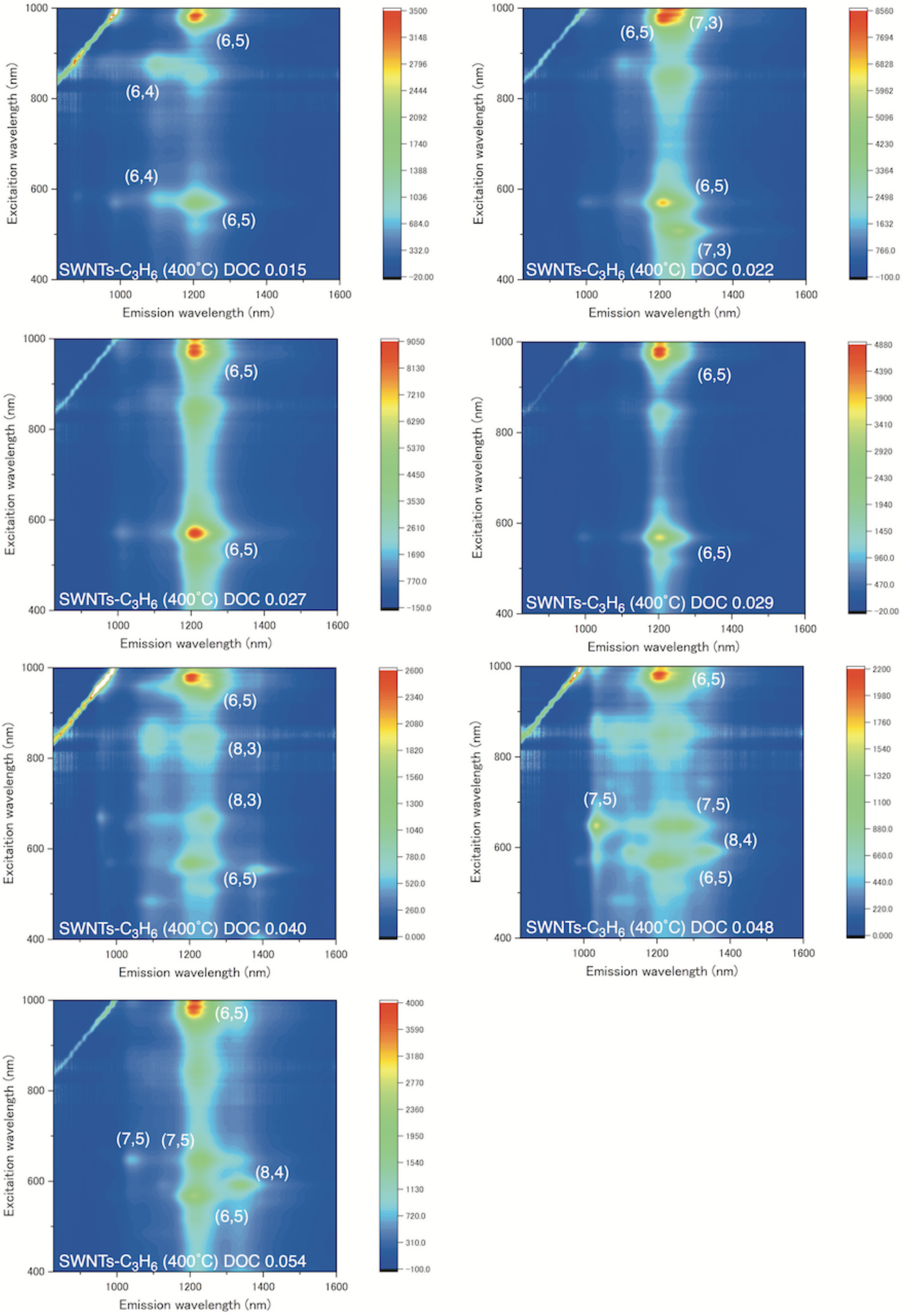

Fig. S18 PL mapping of SWNTs-C_3H_6 (400 ˚C) dispersed in D_2O containing 1 wt.% SC.

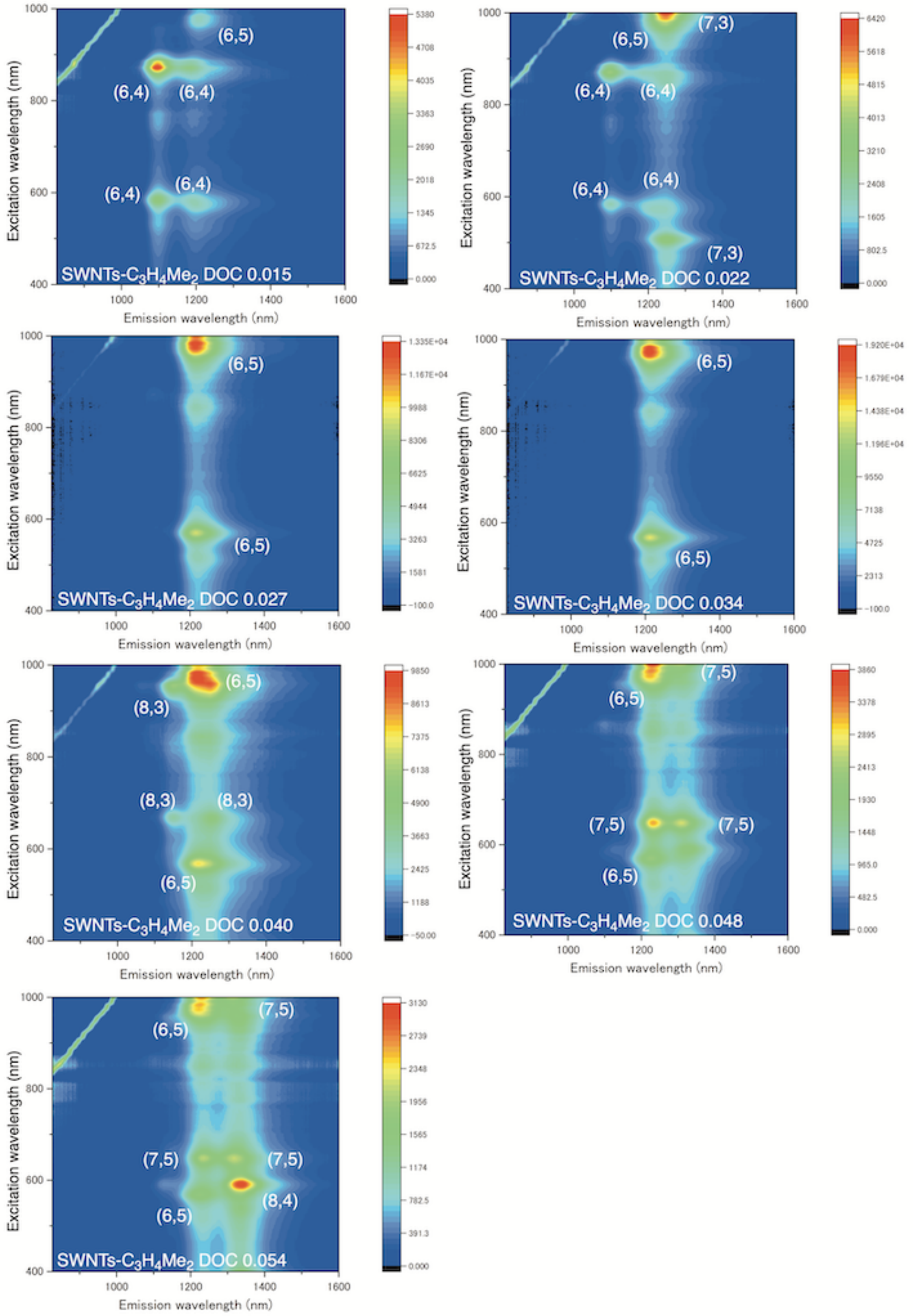

Fig. S19 PL mapping of SWNTs-C$_3$H$_4$Me$_2$ dispersed in D$_2$O containing 1 wt.% SC.

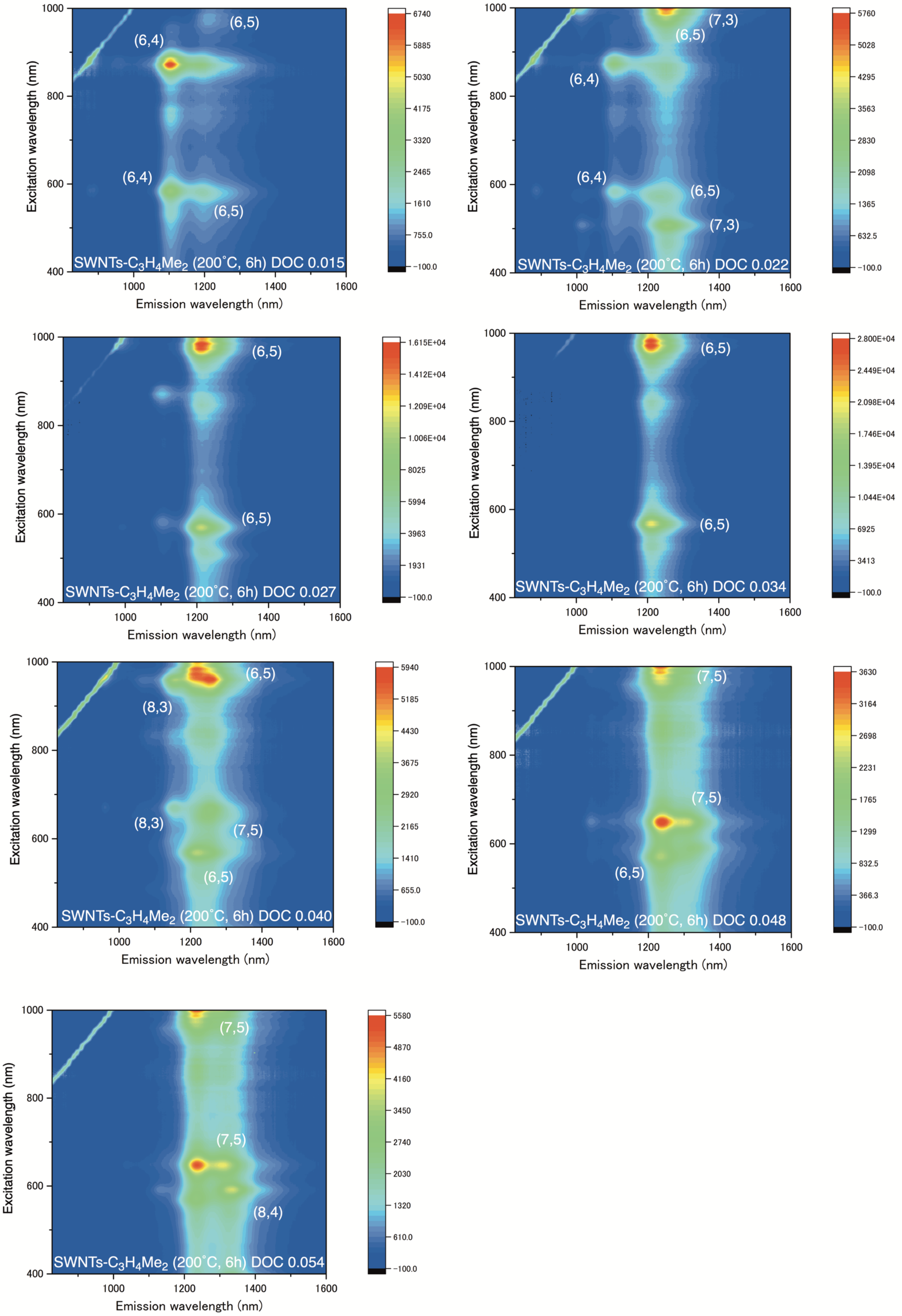

Fig. S20 PL mapping of SWNTs-$C_3H_4Me_2$ (200 ˚C, 6h) dispersed in D_2O containing 1 wt.% SC.

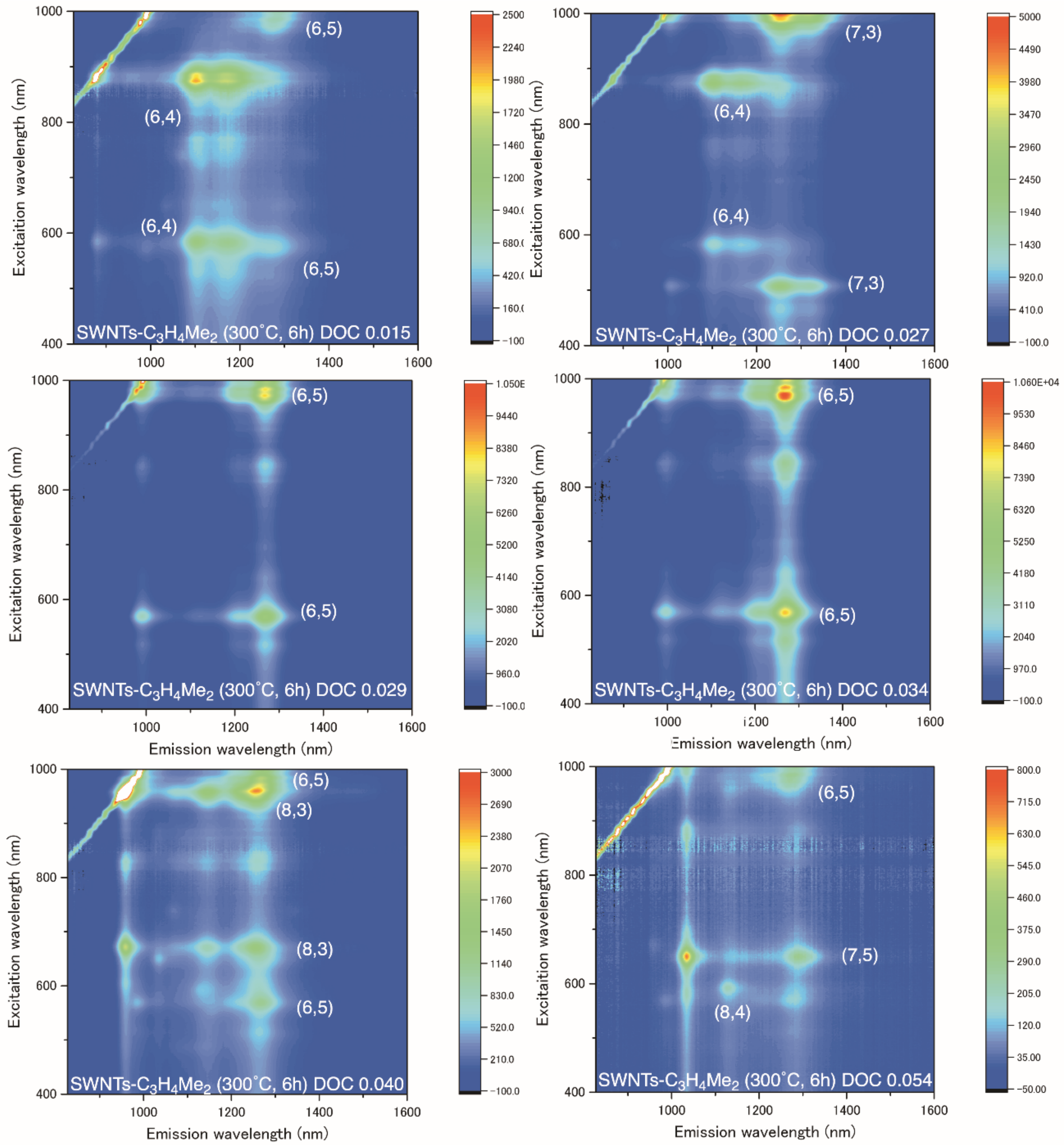

Fig. S21 PL mapping of SWNTs-C$_3$H$_4$Me$_2$ (300 ˚C, 6h) dispersed in D$_2$O containing 1 wt.% SC.

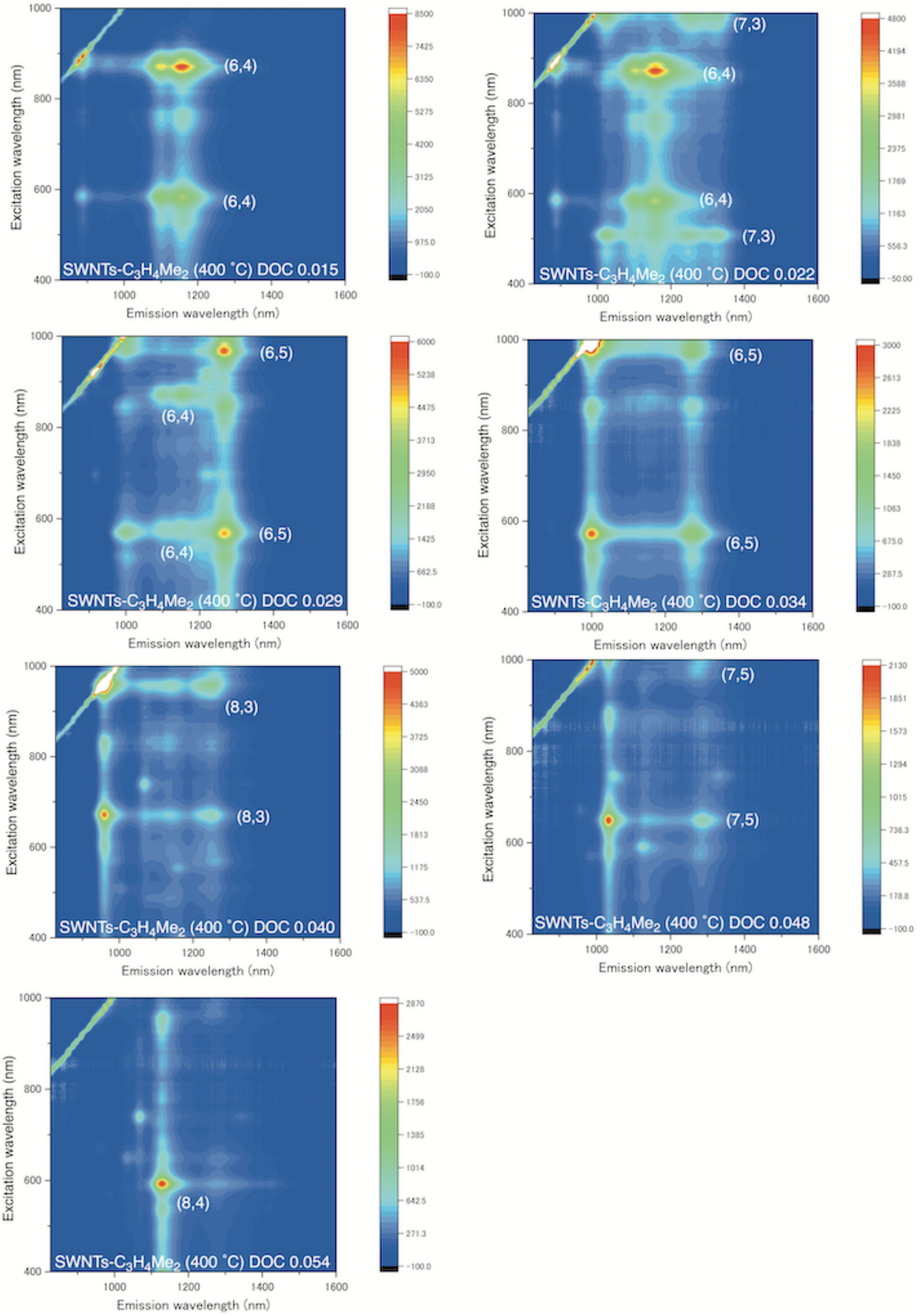

Fig. S22 PL mapping of SWNTs-$C_3H_4Me_2$ (400 ˚C) dispersed in D_2O containing 1 wt.% SC.

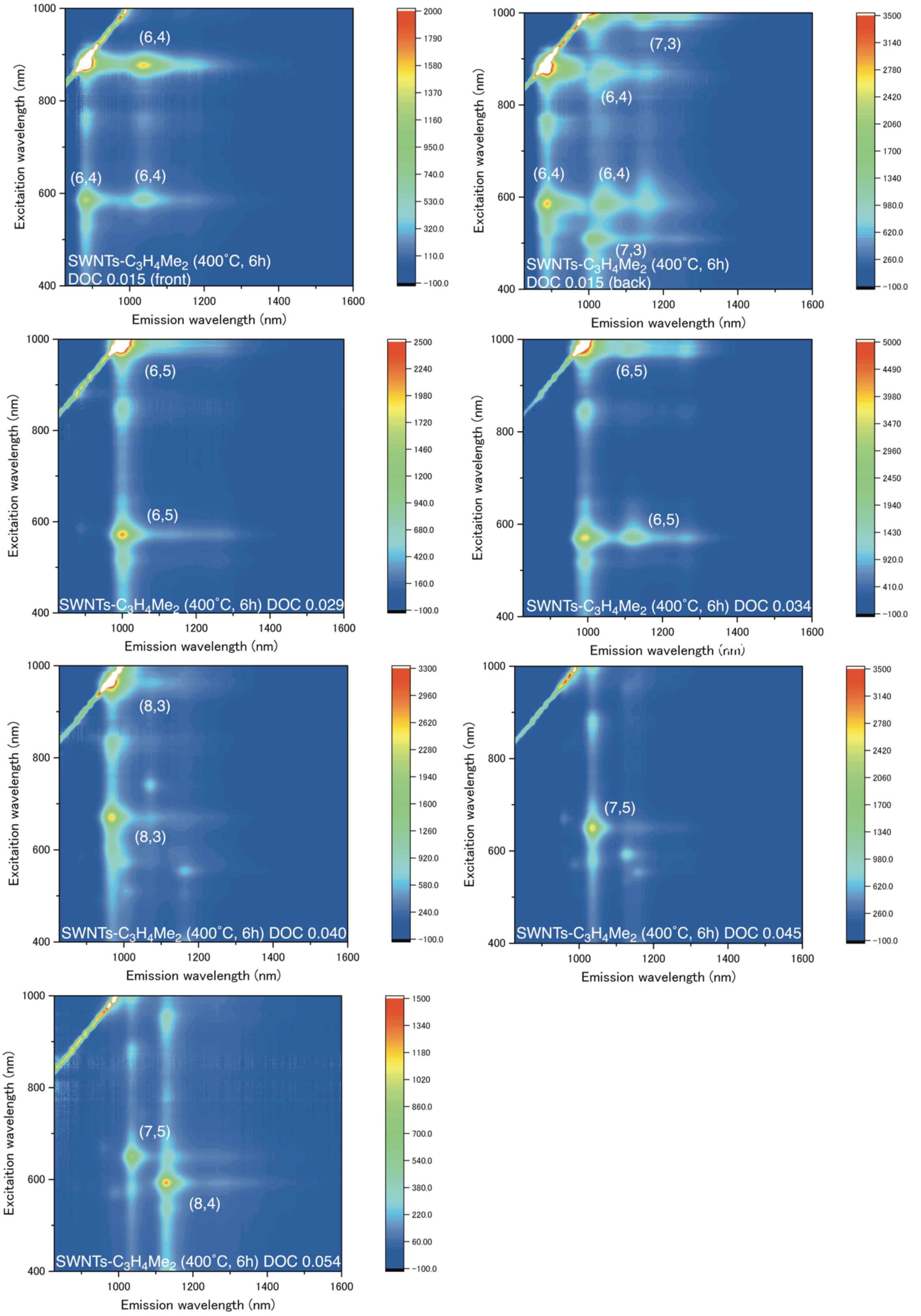

Fig. S23 PL mapping of SWNTs-$C_3H_4Me_2$ (400 ˚C, 6 h) dispersed in D_2O containing 1 wt.% SC.

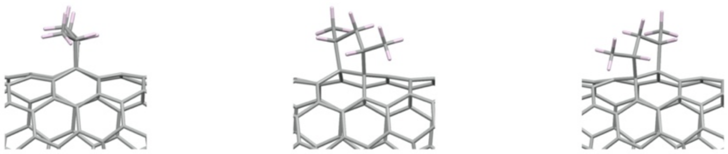

1,2-L_{++} (6,4) *cis*-SWNT-$C_3H_4Me_2$
1,2-L_{+} (6,4) *cis*-SWNT-$C_3H_4Me_2$
1,2-L_{-} (6,4) *cis*-SWNT-$C_3H_4Me_2$

1,2-L_{++} (6,4) *trans*-SWNT-$C_3H_4Me_2$
1,2-L_{+} (6,4) *trans*-SWNT-$C_3H_4Me_2$
1,2-L_{-} (6,4) *trans*-SWNT-$C_3H_4Me_2$

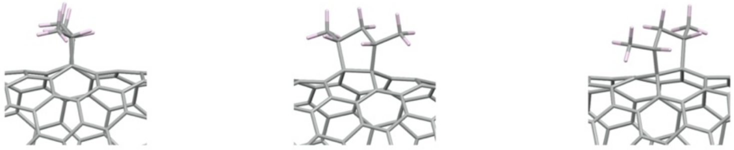

1,2-L_{++} (8,3) *cis*-SWNT-$C_3H_4Me_2$
1,2-L_{+} (8,3) *cis*-SWNT-$C_3H_4Me_2$
1,2-L_{-} (8,3) *cis*-SWNT-$C_3H_4Me_2$

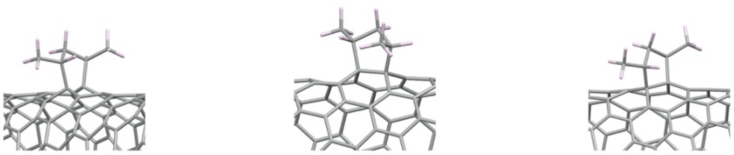

1,2-L_{++} (8,3) *trans*-SWNT-$C_3H_4Me_2$
1,2-L_{+} (8,3) *trans*-SWNT-$C_3H_4Me_2$
1,2-L_{-} (8,3) *trans*-SWNT-$C_3H_4Me_2$

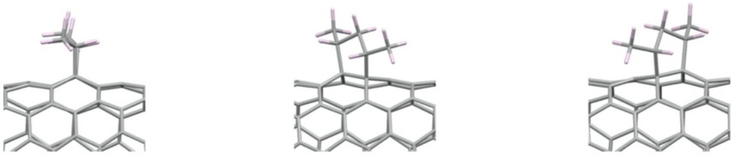

1,2-L_{++} (7,5) *cis*-SWNT-$C_3H_4Me_2$
1,2-L_{+} (7,5) *cis*-SWNT-$C_3H_4Me_2$
1,2-L_{-} (7,5) *cis*-SWNT-$C_3H_4Me_2$

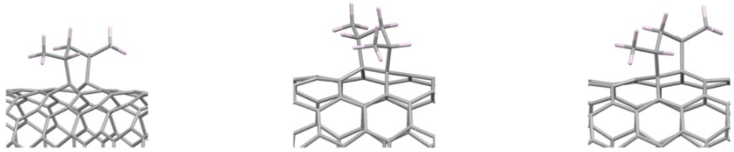

1,2-L_{++} (7,5) *trans*-SWNT-$C_3H_4Me_2$
1,2-L_{+} (7,5) *trans*-SWNT-$C_3H_4Me_2$
1,2-L_{-} (7,5) *trans*-SWNT-$C_3H_4Me_2$

Fig. S24 Partial view of the optimized structures of SWNTs-$C_3H_4Me_2$ at the level of B3LYP/6-31G*.

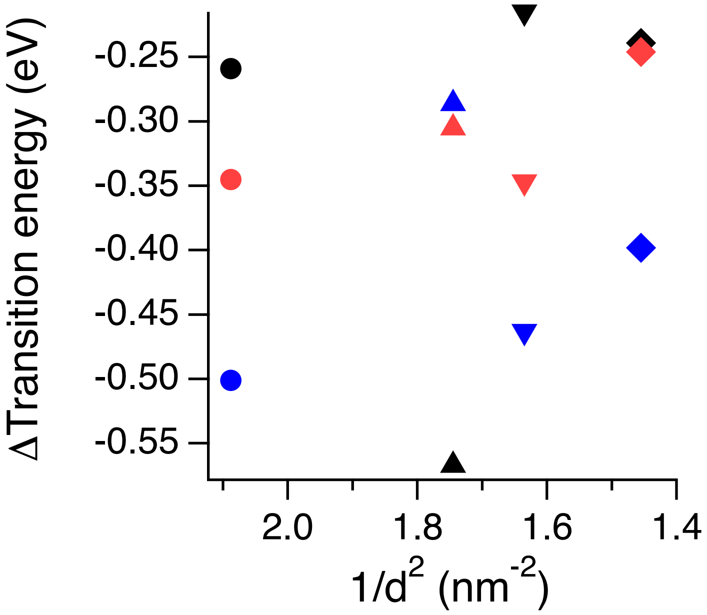

Fig. S25 Calculated transition energy difference between the functionalized and non-functionalized SWNTs (Δtransition energy) as a function of the squared diameter of SWNTs. 1,2-L$_{++}$ binding configuration (red). 1,2-L$_{+}$ binding configuration (black). 1,2-L$_{-}$ binding configuration (blue). *trans*-(6,4) SWNTs-$C_3H_4Me_2$ (●). *trans*-(6,5) SWNTs-$C_3H_4Me_2$ (▲). *trans*-(8,3) SWNTs-$C_3H_4Me_2$ (▼). *trans*-(7,5) SWNTs-$C_3H_4Me_2$ (◆).

Table S1. Relative energies (ΔE, in kcal/mol), transition energies (in eV/nm), and oscillator strength (*f*) of SWNTs-$C_3H_4Me_2$.

Binding configuration	ΔE	Transition energy		Oscillator strength
		eV	nm	f
		(6,4) SWNT-$C_3H_4Me_2$		
1,2-L_{83}-*cis*	4.3	1.416	875	0.266
1,2-L_{83}-*trans*	7.2	1.415	877	0.432
1,2-L_{23}-*cis*	1.6	1.504	825	0.214
1,2-L_{23}-*trans*	0.0	1.501	826	0.175
1,2-L_{-37}-*cis*	4.4	1.253	990	0.811
1,2-L_{-37}-*trans*	6.3	1.259	985	0.797
		(8,3) SWNT-$C_3H_4Me_2$		
1,2-L_{75}-*cis*	3.5	1.296	957	0.556
1,2-L_{75}-*trans*	6.8	1.293	959	0.527
1,2-L_{15}-*cis*	3.1	1.425	870	0.218
1,2-L_{15}-*trans*	0.0	1.425	870	0.234
1,2-L_{-45}-*cis*	3.9	1.173	1057	0.747
1,2-L_{-45}-*trans*	5.6	1.177	1054	0.756
		(7,5) SWNT-$C_3H_4Me_2$		
1,2-L_{85}-*cis*	3.0	1.245	996	0.662
1,2-L_{85}-*trans*	6.2	1.244	996	0.634
1,2-L_{25}-*cis*	1.5	1.255	988	0.265
1,2-L_{25}-*trans*	0.0	1.251	991	0.261
1,2-L_{-35}-*cis*	3.2	1.089	1139	0.858
1,2-L_{-35}-*trans*	5.5	1.092	1136	0.851